

Journal of Thermal Engineering

Web page info: https://jten.yildiz.edu.tr DOI: 10.14744/thermal.0001025



Research Article

Comparative performance of different solar still configurations

P. VELMURUGAN¹®, K. KUMARARAJA²®, R. S. HARISIVASANKARAN¹,³®, S. SARAVANAN¹,∗®

¹Department of Mechanical Engineering, Annamalai University, Annamalainagar, Tamilnadu, 608002, India ²Department of Mechanical Engineering, New Prince Shri Bhavani College of Engineering and Technology, Chennai, Tamilnadu, 600073, India

³Hexaware Technologies, Pallikaranai, Chennai, Tamilnadu, 600129, India

ARTICLE INFO

Article history
Received: 09 August 2024
Accepted: 13 October 2024

Keywords:

Black Cloth; Configuration; DNN; Performance; Solar Still; Water Collected

ABSTRACT

This study evaluates the performance of three solar still configurations: the conventional solar still, the pyramid solar still with fins, and the pyramid solar still with fins covered in black cotton cloth. The variation in absorber plate, glass plate, water temperature, and the quantum of water collected in the attempted configurations was determined at identical conditions. Of the three solar still configurations, the pyramid shaped solar still having fins covered with a black cloth exhibited better efficiency and produced 3.7 liters of potable water. The pyramid shaped solar still having fins closely follows with a water production of three liters. The superior performance is due to the better heat absorption and heat transfer following the enhanced area and the capillary effect of the black cloth. In addition, a deep neural network model with better accuracy, having an R² value of 0.96, was created in the Python environment to predict the glass, absorber, and water temperatures along with the water collected. The novel integration of experimental and artificial intelligence in the optimization of solar still provides room for potential seawater-to-potable-water conversion and is suitable for remote or hilly areas.

Cite this article as: Velmurugan P, Kumararaja K, Harisivasankaran RS, Saravanan S. Comparative performance of different solar still configurations. J Ther Eng 2025;11(6):1729–1740.

INTRODUCTION

Researchers around the world are increasing their focus on developing sustainable and renewable energy, and thereby transforming the world's energy landscape. Of the various renewable energy solutions, solar energy has gained significant attention due to its capability to address the growing energy demand along with mitigating the environmental impact [1]. Though solar energy is employed for numerous applications, solar desalination plays a vital

role, as it provides a viable solution for addressing the acute water shortages in arid regions having limited or no freshwater options [2]. Solar stills, a subset of solar desalination, demonstrated significant success in harnessing solar energy for water purification [3].

Basin type solar stills evaporate the saline water by harnessing the solar energy, followed by the condensation of vapor to yield freshwater [4]. Earlier researchers attempted different modifications, materials, and varied process

This paper was recommended for publication in revised form by Editor-in-Chief Ahmet Selim Dalkilic



^{*}Corresponding author.

^{*}E-mail address: ssvcdm@gmail.com

parameters to augment the performance of the solar stills. Ensafisoroor et al. introduced steps and placed sponges on the basin solar still and successfully increased the water production [5]. Likewise, Hansen et al. used flat, grooved, and fin-shaped absorber plates in an inclined solar still to recover waste heat, resulting in higher water productivity [6]. Goshayeshi and Safaei studied the effect of varying the glass cover's inclination angle (25°, 27.5°, 30°, 32.5°, and 35°) in stepped solar stills and recommended an optimal angle of 32.5° for improved performance [7]. In a related effort, Omara et al. developed a pyramid-shaped solar still with convex cylinders and nanocomposite-based dish absorber plates to achieve greater efficiency [8]. Ahamed et al. attempted phase change material encapsulated fins and thereby successfully enhanced the thermal performance of the basin solar still [9]. Meanwhile, Kabeel et al. employed v-corrugated absorber plates in a tubular solar still and reported improved performance. In addition, they also developed a mathematical model to replicate the operation of the solar still as well [10]. On the other hand, Hameed et al. performed an experimental study on a single slope solar still and correlated the results with the numerical simulation performed using COMSOL. According to their results, both numerical and experimental outcomes are in good agreement with each other [11]. In 2021, Jobrane et al. summarized the research carried out by other researchers on wick-type solar stills, involving variations in geometrical designs, wick arrangements, and integrated heating systems [12].

Few researchers introduced machine learning on predicting the performance of solar stills. Wang et al. successfully applied the Bayesian optimization algorithm to predict the performance of tubular solar stills [13]. Moustafa et al. utilized an artificial neural network (ANN) to forecast the thermal efficiency and water production of solar stills [14]. Similarly, Bahiraei et al. used a hybrid ANFIS model and a PSO-enhanced neural network to predict energy efficiency with improved accuracy [15].

It is inferred that the published literature focused on varying the absorbing surface, condensation enhancement techniques, and geometric modifications to augment the overall performance of a solar still. Likewise, different types of absorber plates and transparent covers are attempted to improve the heat absorption and to curtail the heat losses [16]. In addition, the effect of climatic conditions such as solar radiation [17, 18], ambient temperature [19], and wind speed [20] on the performance of basin solar stills is reported. The present study proposes the integration of fins and black cotton cloth in a pyramid solar still to attain an improved heat transfer and absorption, leading to higher water yield. The use of the machine learning technique (DNN) for predicting the performance of the solar still provides scope for future improvements in system design and optimization with minimum experimentation.

MATERIALS AND METHODS

In this study, three different types of solar stills viz., a conventional solar stills (CSS), a pyramid solar still with fins (PSSF), and a pyramid solar still with fins covered with black cloth (PSSFB), were fabricated using 18-gauge alloy sheets, having a uniform basin area of 1 m². These were designed and uniformly tested at the Department of Mechanical Engineering, Annamalai University, Tamilnadu, India. The dimensions of the stills were 110 cm in length and 110 cm in breadth.

The CSS serves as the reference, whose basin is coated black, covered with a transparent 4 mm thick glass, having transitivity of 88%, and inclined at 11° (based on the location) to maximize the solar exposure. Water is filled to a depth of 1 cm for effective operation. The edges of the transparent glass cover are fixed with a rubber gasket to curtail the losses. The pyramid solar still (Fig. 1: PSSF) retains the basic components of CSS apart from having the pyramid shaped glass cover, fabricated using four glasses having an equal slope. The covers were attached and sealed



Figure 1. Pyramid shaped solar still with fins attached.



Figure 2. Pyramid shaped solar still with fins covered by black cloth.

using silicone sealant. The metallic fins in the pyramid shaped absorber plate are also coated with black paint and positioned at 90°. In the third setup (PSSFB), a layer of black cloth was employed to cover the fins (Fig. 2).

The condensate was collected in a trough located at the base of the glass cover. Thermocouples were positioned at various locations of the solar stills to measure the temperatures of the absorber and glass plates and water. Temperature data were logged using a twelve-channel temperature indicator. A digital thermometer was used to measure the ambient temperature, while the Solar HT kit with a PV204 Solarimeter with an accuracy of $\pm 1~\rm W/m^2$ was utilized to record the solar intensity. The distilled water was collected in a transparent beaker. Experiments were conducted between 09:00 a.m. and 4:00 p.m. over 25 different days from March to May 2024. The variation in glass, absorber, water, and ambient temperatures; solar radiation; and water yield were recorded at an equal interval of 30 minutes.

Subsequent to the experimentation, the obtained data were utilized to develop an artificial intelligence model

employing a deep neural network, which is described below. Of the available data, 70% was used for training the model, and the remaining 30% was equally used for validation and testing on a Windows computer.

Deep Neural Network

A deep neural network is a complex model based on machine learning techniques that comprises several layers interconnected by neurons (Fig. 3). It is employed to learn complicated patterns within large datasets automatically [21]. There are several neurons within each layer of a DNN that transform the input data and refine features in order to make an accurate prediction. Moreover, the model is equipped with advanced optimization techniques and a host of activation functions, hence very effective in predictive analytics [22]. The depth and architecture are critical in DNN, as this generalizes from training data onto unseen examples and thus drives actual performance in deployment.

The accuracy of predicting the responses (temperatures and water collection), with respect to training and testing data, is determined with the aid of three performance

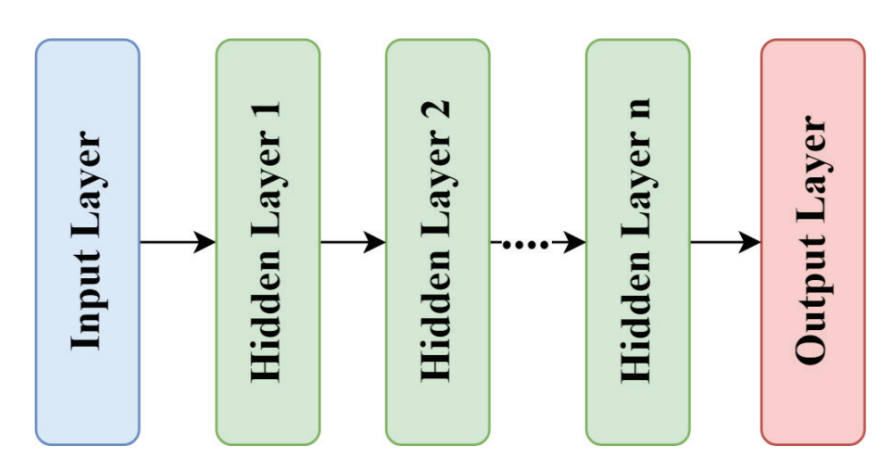


Figure 3. DNN model structure.

metrics: a) Mean Absolute Error (MAE), b) the coefficient of determination (R^2), and c) Mean Absolute Percentage Error (MAPE). MAE represents the average magnitude of errors between predicted and actual values. R^2 indicates the proportion of variance in the actual data explained by the model. MAPE expresses the error as a percentage by averaging the absolute percentage differences between predicted and actual values. These metrics quantify the deviation between predicted and experimental results. The attempted performance measures are calculated by: [23].

$$MAE = \frac{\sum_{j=1}^{n} (Y_k - y_k)}{n} \tag{1}$$

$$MAPE = \frac{\sum_{j=1}^{n} (Y_k - y_k)}{Y_K} \times 100$$
 (2)

$$R^{2} = 1 - \frac{\sum_{k=1}^{n} (Y_{k} - y_{k})^{2}}{\sum (Y_{k} - Y_{k,mean})^{2}}$$
(3)

RESULTS AND DISCUSSION

Variation in Solar Intensity Over Time

The solar intensity (power received from the sun per unit area) is a critical factor influencing the evaporation and condensation process and thereby dictating the overall efficiency and performance of solar stills. Figure 4 illustrates the fluctuations in solar radiation over the daytime. Further, it is observed that a uniform pattern in solar intensity is observed. The solar intensity varies throughout the day due to the rotation of the earth and the position of the sun in the sky [24].

In the early morning hours, the sunlight reaches the earth at a shallow angle, and hence the intensity of solar radiation is lower. Consequently, the solar still absorbs minimal heat, and the evaporation of water is lesser. As the day progresses, the sun rises and reaches higher angle of incidence, leading to a higher concentrated solar intensity. The solar intensity increases, reaching a maximum (829.6 w/m^2) around noon. The occurrence of maximum solar intensity around noon is similar to the studies of Osigbemeh et al [25]. During this period the efficiency of the solar still is higher following the availability of maximum thermal energy for evaporation.

Post noon, the sun starts to descend, and hence the solar intensity declines. The decline in solar intensity gradually decreases the rate of evaporation in the afternoon, and hence the performance of the solar still reduces significantly. By late afternoon and into the evening, the solar intensity greatly reduces, and consequently, the evaporation rate. The fluctuation in solar intensity emphasizes the significance of modifications in the solar still design to harness solar energy effectively.

Variation in Temperatures

The effect of design modifications on the average absorber plate, glass plate, and water temperatures obtained across the three solar still configurations are illustrated in Figs. 5-7. The temperatures in all three solar still configurations rise from 10:00 hours and reach the maximum between 12:00 and 13:00 hours, and then a gradual decrease is witnessed in the afternoon. Higher temperatures during the midday impart more thermal energy to water, accelerating the evaporation of water [26].

In the conventional solar still (CSS), the maximum temperature of the absorber plate reaches around 68 °C when the solar radiation is peaking (Fig. 5). The maximum temperature supports the evaporation process, as the available heat is absorbed by the plate and the same is transferred to the water medium. Subsequently, the water temperature (Fig. 6) in the CSS lags behind the absorber plate temperature (66 °C). This phenomenon is consistent with the studies of Peng and Sharshir [27]. The glass plate, otherwise termed the condensation surface, maintains a lower

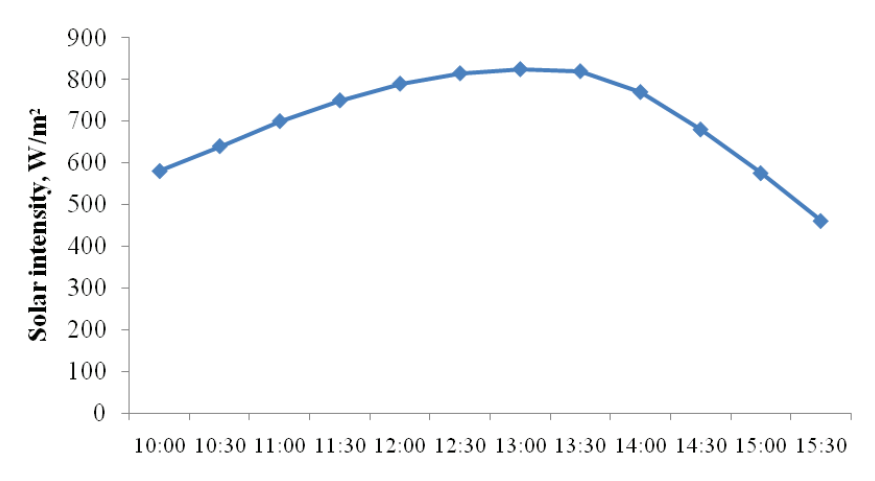


Figure 4. Variation in solar intensity over time.

temperature (Fig. 7), around 55-57 °C, due to its exposure to the ambient air and the evaporative cooling effect [28]. The temperature gradient between the water and the glass plate is crucial for maximizing the condensation rate, thus improving the water production.

However, the introduction of fins in a pyramid shaped solar still (PSSF) improves the overall heat transfer area, promoting better heat distribution to result in higher thermal performances than the CSS. The fins, attached to the absorber plate, facilitate more efficient heat distribution throughout the water [29]. In addition, the pyramid shape promotes concentration of solar radiation to amplify the absorber plate temperature. This modification raises the absorber plate temperature to 73-77 °C (Fig. 5). Consequently, the water temperature also rises, reaching 74 °C (Fig. 6), as the fins allow more heat to be absorbed and transferred. The glass plate temperature in this design reaches 60 °C (Fig. 7), but the increased evaporation rate leads to a higher overall productivity (detailed in the next section).

The third solar still configuration, pyramid shaped solar still with fins covered by black cloth, displays the maximum

thermal performance. The usage of black cloth increases the absorptivity, minimizes the reflective losses, and maximizes the heat retention [30]. As a result, the absorber plate reaches a temperature as high as 75-78 °C (Fig. 5), higher than the other two attempted solar still configurations. Consequently, the water temperature increases to 75 °C (Fig. 6). The difference in temperature between the water and the glass plate, reaching nearly 64 °C (Fig. 7), significantly improves the evaporation and condensation rates. The black cloth-covered fins make sure that the heat is distributed uniformly and retained for a longer duration, leading to a higher temperature in the water. Singh et al [31] opined that enhancing the surface area enhances the absorber plate temperature, consistent with the present study. It is concluded that the variations in the absorber plate, water, and glass plate temperatures among the three configurations illustrate the profound influence of design modifications on solar still performance. Though the conventional pyramid shaped still is effective, the addition of fins and the use of black cloth over the fins provide significant improvements in attaining higher temperatures, leading to increased potable water production (discussed below).

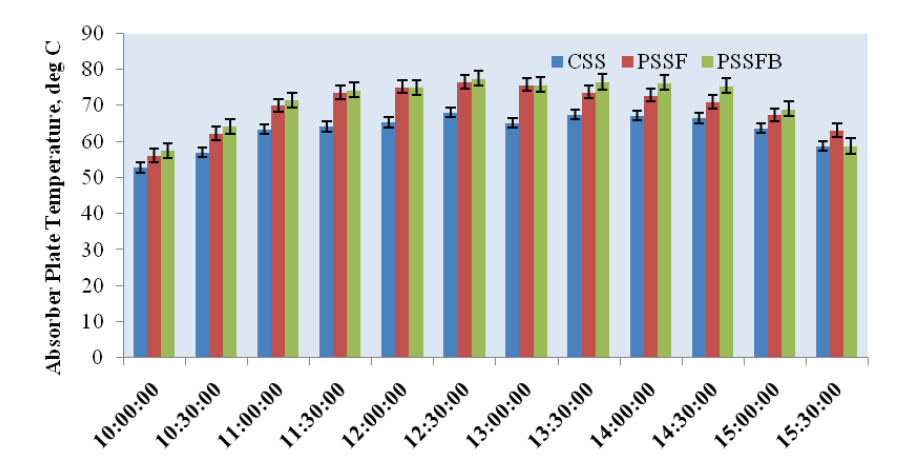


Figure 5. Variation in absorber plate temperature over time.

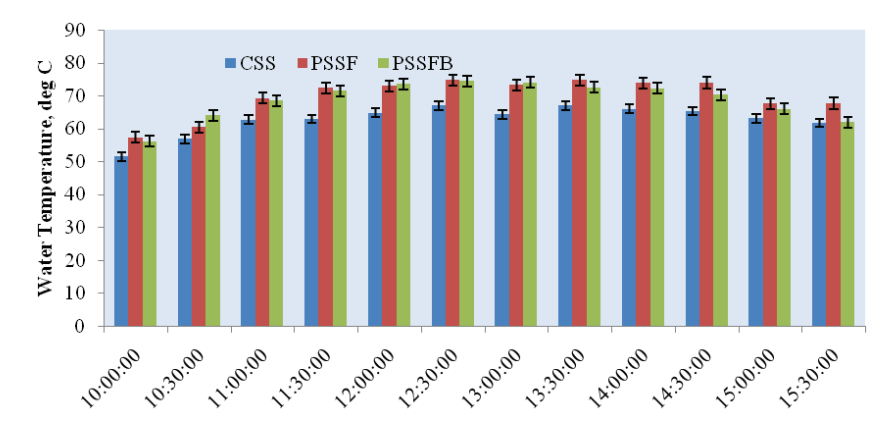


Figure 6. Variation in water temperature over time.

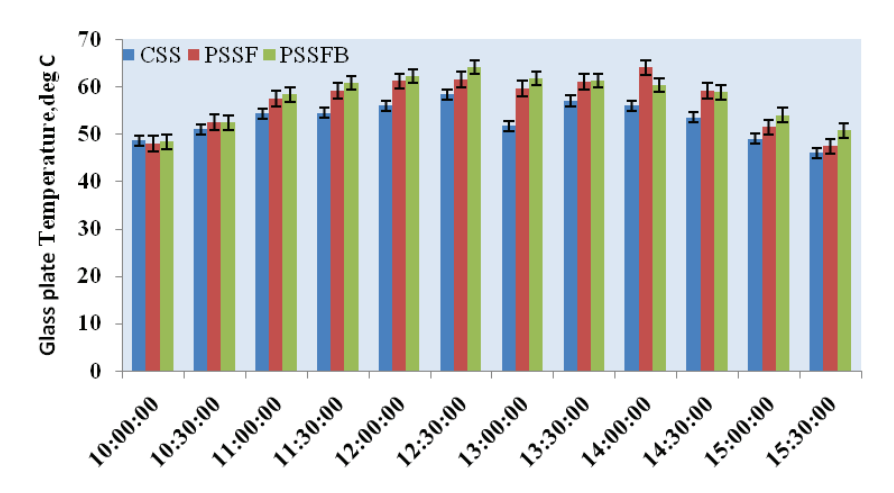


Figure 7. Variation in glass plate temperature over time.

Water Collected

The conventional solar still (CSS) traps the solar energy through a transparent cover, which heats the water prevailing inside. Subsequently, the water evaporates and condenses on the cooler surface of the cover and is collected as distilled water. The CSS produces around 2.3 liters of water per day under optimal conditions (Fig. 8). However, the pyramid shaped solar still with fins (PSSF) yields 3 liters of water, 30% more than the CSS. The increased water yield is due to the higher surface area exposure to sunlight created by the geometrical modification i.e. the pyramid shaped absorber plate, as reported by Hammoodi et al [32]. The surface area and water evaporation rates of the solar still are further increased by the attachment of fins. The fins increase the temperature of the water and the inner surfaces of the solar still, yielding more water. The presence of fins aids in even distribution of heat across the solar still, suppressing the temperature gradients within the still. The fins guide the water towards the collection trough as well.

The maximum water collection (3.7 liters), which is 23 % more than the PSSF is obtained for the pyramid-shaped solar still with fins covered with black cloth (PSSFB) configuration. The 23% increase is attributed to the presence of black cloth which harnesses more solar radiation to obtain superior evaporation and collection efficiency. In addition, the capillary effect of drawing water upwards and spreading it evenly over a larger surface area supports the phenomenon. As the water vapor rises, it condenses on the transparent glasses of the still, resulting in a higher water production. The dual effect of improved thermal absorption and efficient water distribution makes the PSSFB an effective modification for achieving higher thermal performance and more water collection.

Energy Balance

In a solar still, energy balance accounts for heat transfer between the absorber, glass, and water through radiation, convection, and conduction processes. These mechanisms

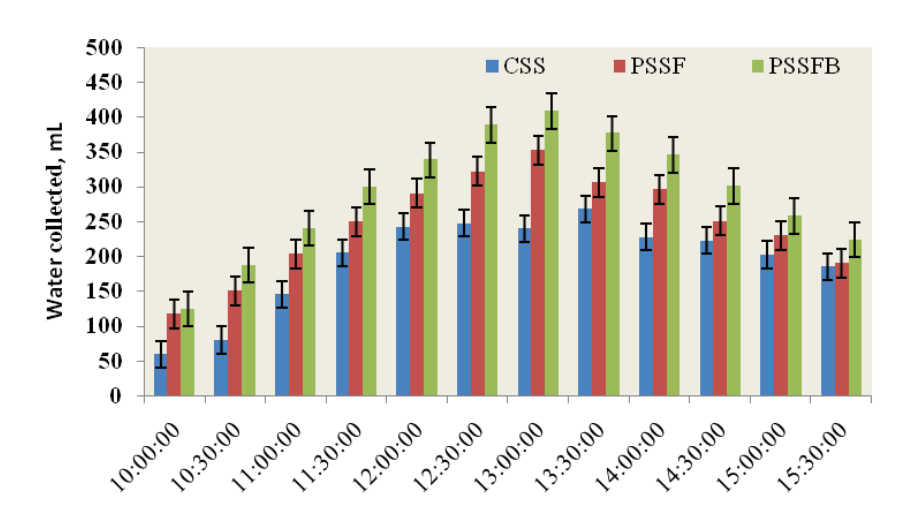


Figure 8. Water collected during day time.

regulate the thermal dynamics essential for efficient water evaporation and condensation. The convective heat transfer between water and glass cover [33]

$$q_{c(w-g)} = h_{c(w-g)} A_w (t_w - t_g)$$
 (4)

$$h_{c(w-g)} = 0.884 [(t_w - t_g) + \{(p_w - p_g)t_w/(268.90 \times 10^3 - p_w)\}]^{1/3}$$
 (5)

$$p_w = e^{\{25.317 - [5144/(t_w + 273)]\}}$$
 (6)

$$p_q = e^{\{25.317 - [5144/(t_g + 273)]\}} \tag{7}$$

Similarly, heat transfer by radiation between water and glass cover [33]

$$q_{r(w-g)} = h_{r(w-g)} A_w (t_w - t_g)$$
(8)

$$h_{r(w-g)} = \varepsilon_{effective} \sigma(t_w^2 + t_g^2)(t_w + t_g)$$
 (9)

$$\varepsilon_{effective} = 1/[(1/\varepsilon_w) + (1/\varepsilon_g) - 1]$$
 (10)

The heat transfer between water and glass cover by evaporation [33]

$$q_{e(w-g)} = h_{e(w-g)} A_w (t_w - t_g)$$
 (11)

$$h_{e(w-g)} = 16.237 \times 10^{-3} h_{c(w-g)} \big[\big(p_w - p_g \big) / \big(t_w - t_g \big) \big] \ (12)$$

Radiation heat transfer between glass cover and atmosphere [33]

$$q_{r(g-a)} = h_{r(g-a)} A_g (t_g - t_a)$$
 (13)

$$h_{r(g-a)} = \varepsilon_g \sigma \left[t_g^4 - t_{sky}^4 \right] / (t_g - t_a)$$
 (14)

$$t_{sky} = t_a - 6 \tag{15}$$

Convective heat transfer from glass cover to atmosphere [33]

$$q_{c(q-a)} = h_{c(q-a)} A_q (t_q - t_a)$$
 (16)

$$h_{c(g-a)} = 5.7 + 3.8V_a \tag{17}$$

Convective mode of heat transfer between basin and water [33]

$$q_{c(b-w)} = h_{c(b-w)} A_w (t_b - t_w)$$
(18)

The yield of the solar still or the amount of water condensed on the inner surface of the glass

$$m_{e(w-g)} = [q_{e(w-g)}/h_{fg}] \times 3600$$
 (19)

Uncertainty Analysis

The accuracy and precision of measurements are influenced by various factors, including the selection of instruments, calibration, testing conditions, observations, environmental factors, readings, and test design [34]. To ensure the tests are properly conducted, an uncertainty analysis is performed. Table 1 lists the instruments used in this study, along with their model, accuracy, and operating range. The smallest potential error for each instrument is calculated by dividing the smallest measurable reading, the minor meter reading, by the lowest possible output value. This calculation yields the instrument's minimum possible error.

The uncertainties of the measuring instruments employed in the study are determined using the equation provided in Ref. [34].

Based on the uncertainty analysis, the total uncertainty of the measuring instruments in this study is found to be within $\pm 1.582\%$.

PREDICTION BY DNN MODEL

The DNN model was trained with the temperatures and water yield data collected during the experimental days. By varying the number of hidden layers and the quantity of neurons in the hidden layers, numerous models were constructed. The range of hyperparameters attempted and the optimal neurons in each hidden layer are shown in Table 2.

Table 1. Instruments employed along with accuracy and range

S. No	Instrument	Model	Accuracy	Range
1.	Anemometer	amiciSense GM816	±5%	0-30 ms
2.	Thermocouple	K-type	±1%	0-100°C
3.	Measuring beaker	1L	±10 Ml	0-1.000mL
4.	Solarimeter	PV204	$\pm 1~Wm^2$	0-5000 Wm ²

Table 2. Hyperparameters tuned

Parameters	Range	Optimal value
No. of dense layers	1 to 6	3
No. of units in layer 1	1 to 1000	835
No. of units in layer 2	1 to 1000	635
No. of units in layer 3	1 to 1000	769

Table 3. Optimizer parameters range

Parameters	Range
Learning rate	1e-3 to 1e-1
Decay	1e-3 to 1e-1

Table 4. Performance metrics

R-Square	MAE	MAPE	MSE
0.9601	1.1986	0.8978	0.0796

The optimum neurons were determined by employing the Adam optimizer, as recommended by Saravanan et al [35]. The learning rates and decays of the Adam optimizer are presented in Table 3.

A scatter plot comparing the actual and predicted temperatures, as well as the amount of water collected, provides valuable insights into the model's accuracy (Figs. 9-12). In the scatter plot for both temperatures and water collected, a larger proportion of experimental data scatter around the diagonal line. The prevalence of data points concentrated in the closer proximity of the diagonal line indicates the existence of a strong correlation between DNN prediction and experimental outcomes. The strong correlation of predicted values by the DNN model indicates higher accuracy [36]. In this model, only a small number of experimental conditions deviate from the median, resulting in a high R² value of 0.96, demonstrating a strong goodness of fit. Table 4 presents the performance metrics for the DNN model's accuracy. With a Mean Absolute Error (MAE) of 1.1986, a Mean Absolute Percentage Error (MAPE) of 0.8978, a Mean Square Error (MSE) of 0.0796, and a high R² value of 0.9601, the DNN model shows a strong alignment with the experimental results. Therefore, the deep neural network model is recommended for predicting temperatures and water collection in a solar still.

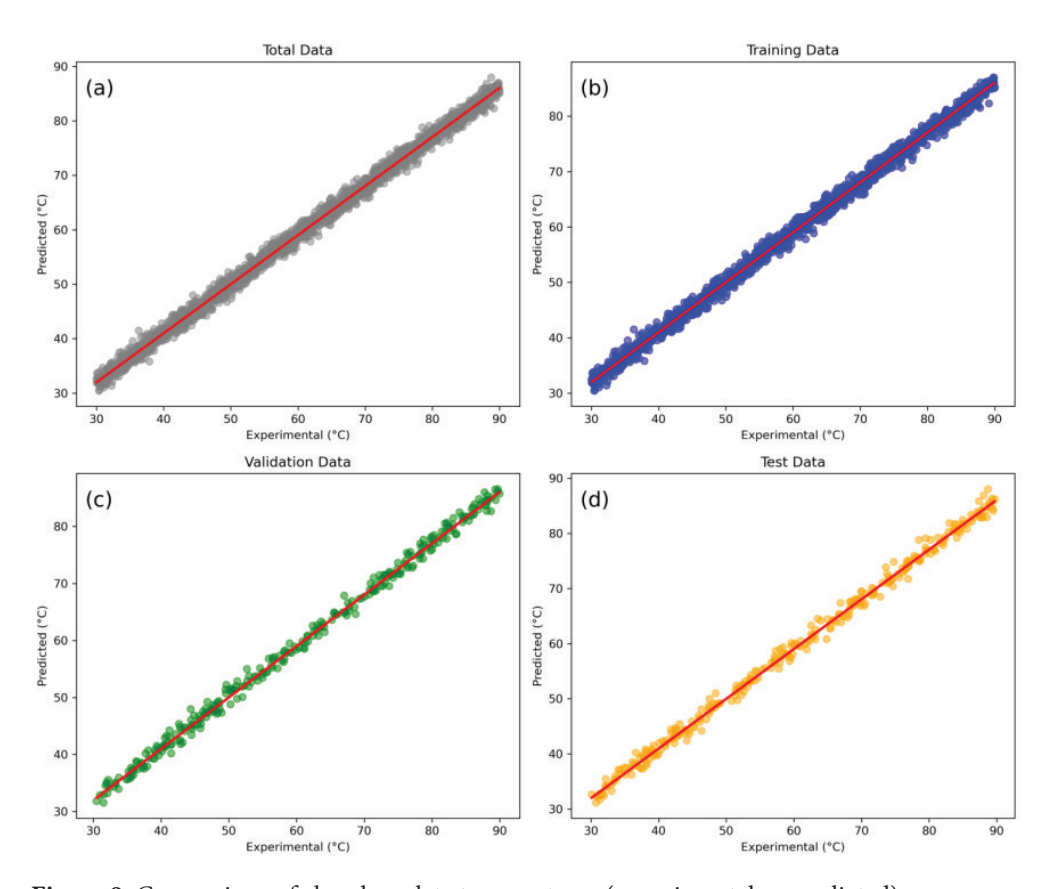


Figure 9. Comparison of absorber plate temperatures (experimental vs predicted).

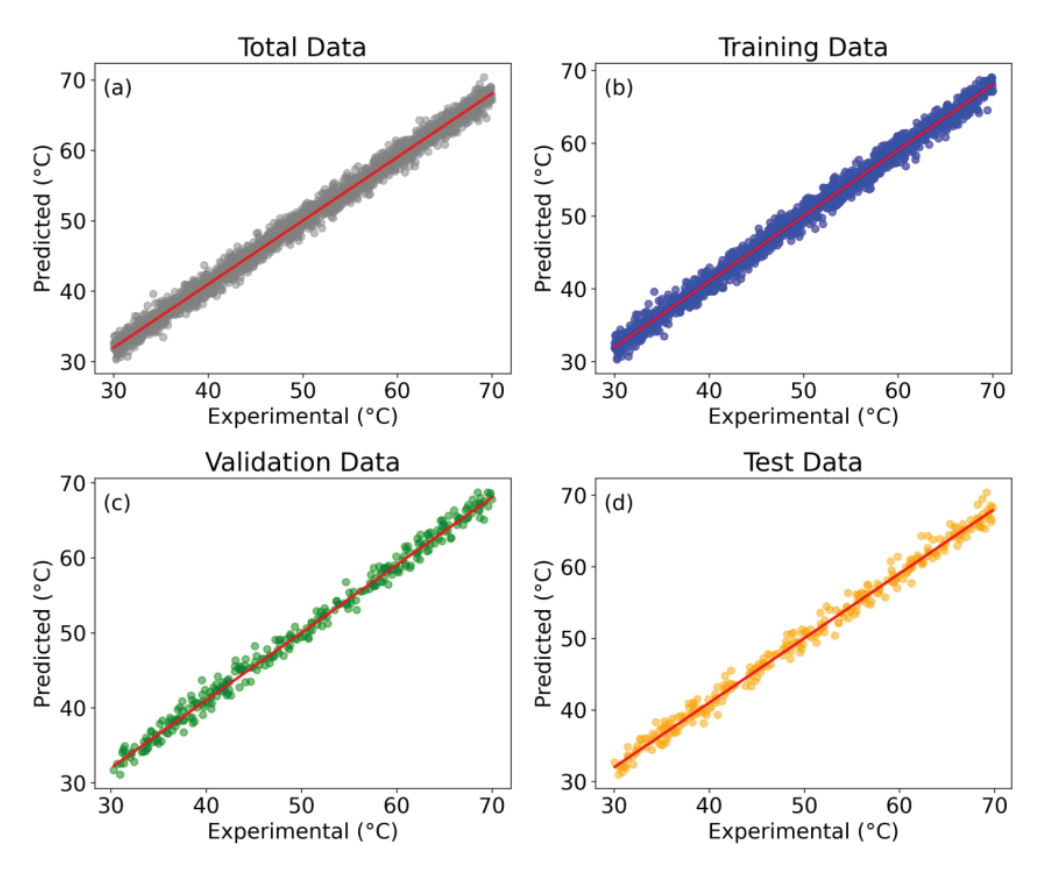


Figure 10. Comparison of glass plate and water temperatures (experimental vs predicted).

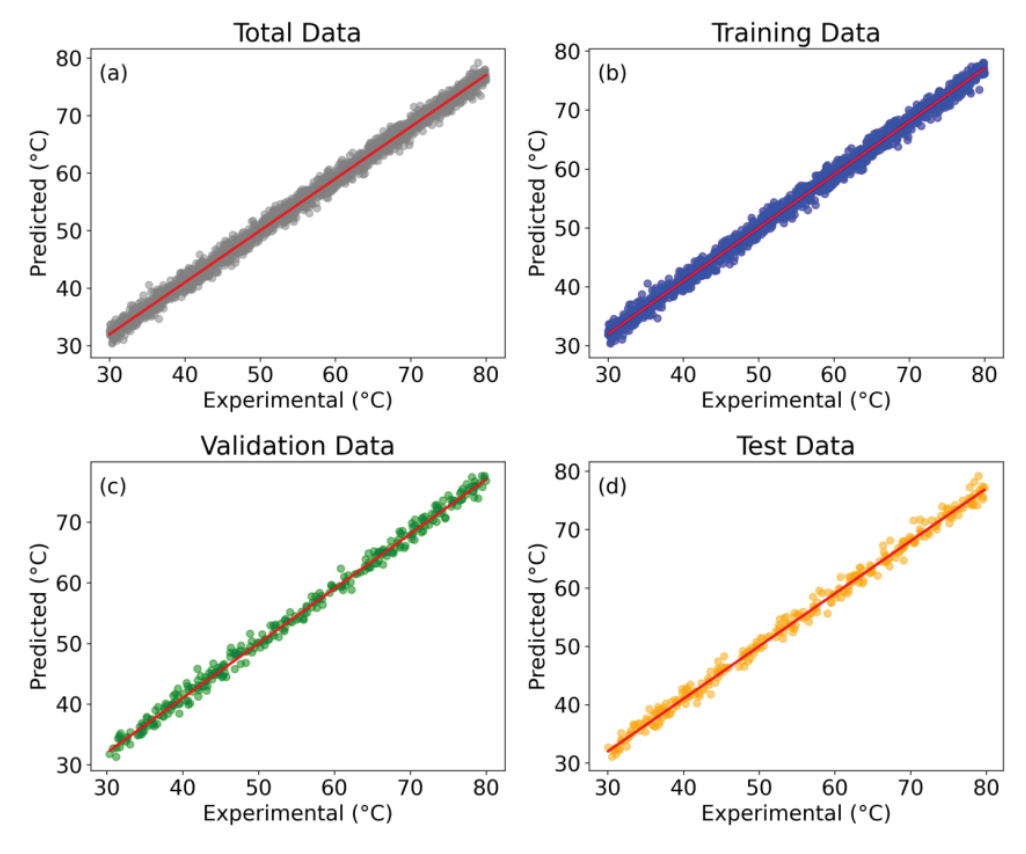


Figure 11. Comparison of water temperatures (experimental vs predicted).

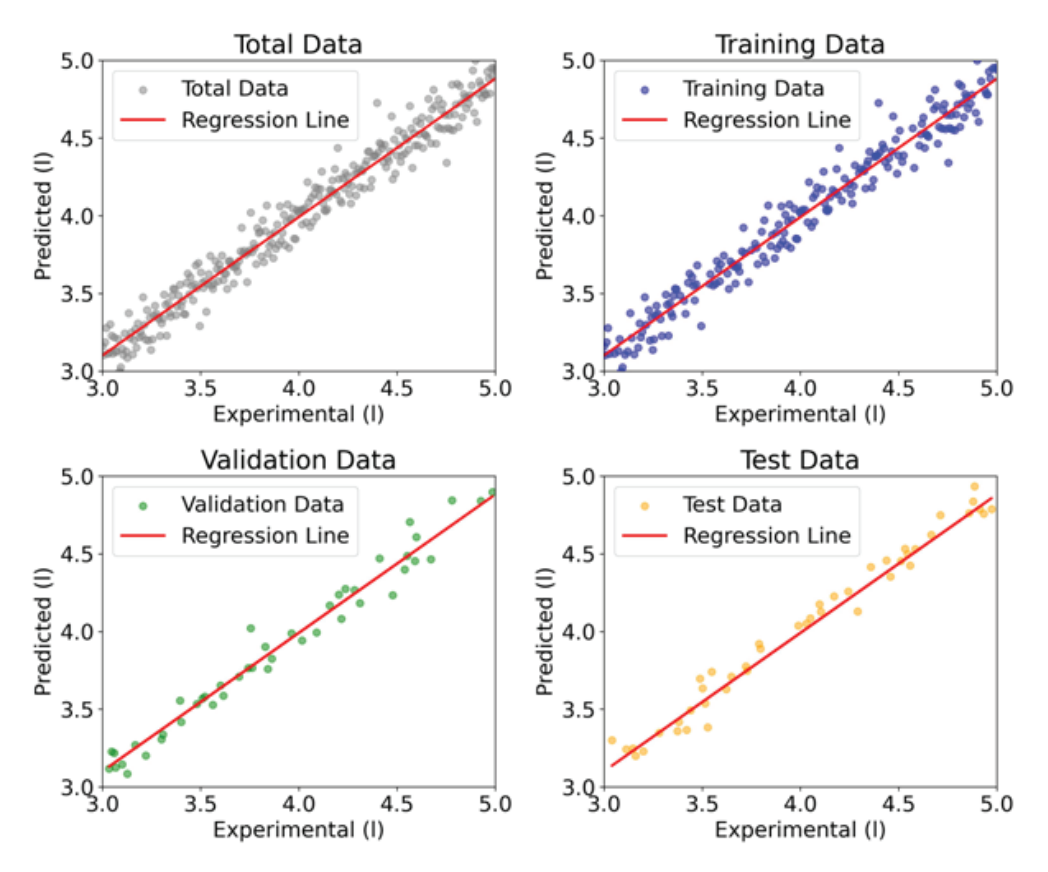


Figure 12. Comparison of water collected experimental vs predicted.

CONCLUSION

The salient conclusions from this novel experimental study on the fabrication and testing of three solar still configurations are as follows:

- 1. The surface modifications in the pyramid shaped absorber plate with fins improve the absorber plate, water, and glass temperatures.
- 2. The employment of fins augments the heat transfer area, and covering the fins by a black cloth cover enhances heat retention and improves the evaporation rate.
- 3. The combined effect of the pyramid shape, fins, and use of black cloth cover results in the highest water collection among the three attempted configurations, highlighting their capability to effectively address acute water shortages.
- 4. The water collected in the solar still having both fins and the black cloth model is nearly twice that of the conventional solar still. The pyramid shaped solar still with fins attains 33% more efficiency than the conventional solar still.
- 5. The Deep Neural Network model is capable of predicting the temperature and water collected in a solar still with an accuracy of 96%.

NOMENCLATURE

A_g	Area of glass cover
$A_{\rm w}$	Absorber Plate area
CSS	Conventional Solar Still
DNN	Deep Neural Network

Heat transfer coefficient due to convection $h_{c(b-w)}$ (basin-water)

Convective heat $h_{c(g-a)}$ transfer coefficient cover-atmosphere)

Convective heat transfer coefficient (water-glass cover)

Evaporative heat transfer coefficient (water-glass $h_{e(w-g)}$ cover)

Latent heat of vaporization h_{fg}

Radiation heat transfer coefficient (glass cover $h_{r(g-a)}$ and atmosphere)

Radiation heat transfer coefficient (glass cover $h_{r(w-g)}$ and water)

MAE Mean Absolute Error

MAPE Mean Absolute Percentage Error Water vapour condensation rate $m_{e(w-g)}$

Partial pressures of vapour at the glass surface $\begin{array}{c} p_g \\ PSSF \end{array}$

Pyramid Solar Still with Fins

PSSFB Pyramid Solar Still with Fins and Black Cloth p_{w} Partial pressures of vapour at the water surface

$q_{c(b-w)}$	Convective mode of heat transfer (basin-water)
$q_{c(g-a)}$	Convective heat transfer (glass cover-atmosphere)
$q_{c(w-g)}$	Convective heat transfer (water-glass cover)
$q_{e(w-g)}$	Evaporative heat transfer (water-glass cover)
$q_{r(g-a)}$	Heat transfer by radiation (glass cover-atmosphere)
$q_{r(w-g)}$	Heat transfer by radiation (water and glass cover)
R^2	Coefficient of determination
t_a	Ambient temperature
t_g	Temperature of glass cover
$t_{\rm sky}$	Sky temperature
$t_{\rm w}$	Temperature of water
Y_k	Actual value
y_k	Predicted value
Y_{k_mean}	Mean actual value
$\varepsilon_{ m effective}^{-}$	Effective emittance (glass cover-water surface)
$\epsilon_{ m g}$	Upper glass emissivity
ε_{w}	Lower glass emissivity

AUTHORSHIP CONTRIBUTIONS

Authors equally contributed to this work.

Stefan-Boltzmann constant

DATA AVAILABILITY STATEMENT

The authors confirm that the data that supports the findings of this study are available within the article. Raw data that support the finding of this study are available from the corresponding author, upon reasonable request.

CONFLICT OF INTEREST

The author declared no potential conflicts of interest with respect to the research, authorship, and/or publication of this article.

ETHICS

There are no ethical issues with the publication of this manuscript.

STATEMENT ON THE USE OF ARTIFICIAL INTELLIGENCE

Artificial intelligence was not used in the preparation of the article.

REFERENCES

- [1] Salhi H, Hadjira A, Jamil B. Statistical analysis of the solar diffuse fraction radiation using regression analysis of longitudinal data in India. J Therm Eng 2023;9:776-785. [CrossRef]
- [2] Mehta P, Bhatt N, Bassan G, Said Z, ElCheikh A. Exploring stepped solar still developments with a case study for potable water provision in salt farming regions. Sustain Energy Technol Assess 2024;64:103700. [CrossRef]

- [3] El-Sebaii AA, El-Bialy E. Advanced designs of solar desalination systems: a review. Renew Sust Energ Rev 2015;49:1198-1212. [CrossRef]
- [4] Das D, Bordoloi U, Kalita P, Boehm RF, Kamble AD. Solar still distillate enhancement techniques and recent developments. Groundw Sustain Dev 2020;10:100360. [CrossRef]
- [5] Ensafisoroor H, Khamooshi M, Egelioglu F, Parham K. An experimental comparative study on different configurations of basin solar still. Desalin Water Treat 2016;57:1901-1916. [CrossRef]
- [6] Hansen RS, Murugavel KK. Enhancement of integrated solar still using different new absorber configurations: an experimental approach. Desalination 2017;422:59-67. [CrossRef]
- [7] Goshayeshi HR, Safaei MR. Effect of absorber plate surface shape and glass cover inclination angle on the performance of a passive solar still. Int J Numer Methods Heat Fluid Flow 2020;30:3183-3198. [CrossRef]
- [8] Omara ZM, Alawee WH, Mohammed SA, Dhahad HA, Abdullah AS, Essa FA. Experimental study on the performance of pyramid solar still with novel convex and dish absorbers and wick materials. J Clean Prod 2022;373:133835. [CrossRef]
- [9] Ahmed ME, Abdo S, Abdelrahman MA, Gaheen OA. Finned-encapsulated PCM pyramid solar still

 experimental study with economic analysis. J
 Energy Storage 2023;73:108908. [CrossRef]
- [10] Kabeel AE, Harby K, Abdelgaied M, Eisa A. Performance improvement of a tubular solar still using V-corrugated absorber with wick materials: numerical and experimental investigations. Sol Energy 2021;217:187-199. [CrossRef]
- [11] Hameed HG, Diabil HAN, Al-Moussawi MA. A numerical investigation of the enhancement of single-slope single-basin solar still productivity. Energy Rep 2023;9:484-500. [CrossRef]
- [12] Jobrane M, Kopmeier A, Kahn A, Cauchie HM, Kharroubi A, Penny C. Internal and external improvements of wick type solar stills in different configurations for drinking water production a review. Groundw Sustain Dev 2021;12:100519. [CrossRef]
- [13] Wang Y, Kandeal AW, Swidan A, Sharshir SW, Abdelaziz GB, Halim MA, et al. Prediction of tubular solar still performance by machine learning integrated with Bayesian optimization algorithm. Appl Therm Eng 2021;184:116233. [CrossRef]
- [14] Moustafa EB, Hammad AH, Elsheikh AH. A new optimized artificial neural network model to predict thermal efficiency and water yield of tubular solar still. Case Stud Therm Eng 2022;30:101750. [CrossRef]
- [15] Bahiraei M, Nazari S, Safarzadeh H. Modeling of energy efficiency for a solar still fitted with thermoelectric modules by ANFIS and PSO-enhanced neural network: a nanofluid application. Powder Technol 2021;385:185-198. [CrossRef]

- [16] Shatar NM, Sabri MFM, Salleh MFM, Ani MH. Energy, exergy, economic, environmental analysis for solar still using partially coated condensing cover with thermoelectric cover cooling. J Clean Prod 2023;387:135833. [CrossRef]
- [17] Sahu SK, Natarajan SK, KAS, Suraparaju SK. Experimental investigation of a solar still combined with phase change material (RT58) in southern India climatic conditions. Proc Inst Mech Eng C J Mech Eng Sci 2023;237:2635-2646. [CrossRef]
- [18] Elsheikh A, Hammoodi KA, Ibrahim A, Mourad AHI, Fujii M, Abd-Elaziem W. Augmentation and evaluation of solar still performance: a comprehensive review. Desalination 2023;555:117239. [CrossRef]
- [19] Alshqirate A, Awad AS, Al Alawin A, Essa MA. Experimental investigation of solar still productivity enhancement of distilled water by using natural fibers. Desalination 2023;553:116487. [CrossRef]
- [20] Abdullah AS, Panchal H, Alawee WH, Omara ZM. Methods used to improve solar still performance with generated turbulence for water desalination detailed review. Results Eng 2023;17:101251. [CrossRef]
- [21] Liu W, Wang Z, Liu X, Zeng N, Liu Y, Alsaadi FE. A survey of deep neural network architectures and their applications. Neurocomputing 2017;234:11-26. [CrossRef]
- [22] Abdou MA. Literature review: efficient deep neural networks techniques for medical image analysis. Neural Comput Appl 2022;34:5791-5812.
- [23] Salhi H, Belkhiri L, Tiri A. Evaluation of diffuse fraction and diffusion coefficient using statistical analysis. Appl Water Sci 2020;10:1-12. [CrossRef]
- [24] Miroshnichenko L. Main characteristics of the sun. In: Solar-Terrestrial Relations: From Solar Activity to Heliobiology. Cham: Springer Int Publ; 2020. p. 7-20. [CrossRef]
- [25] Osigbemeh MS, Asaolu OS, Nwachukwu AN. Sustainable solar power from wall mounted photo-voltaics. Energy Syst 2023;14:1007-1022. [CrossRef]
- [26] Rahul P, Ramanathan S, Dhivagar R, Karthi P, Manivel M. A review on solar desalination techniques using vacuum technology. Proc Inst Mech Eng C J Mech Eng Sci 2023;237:3086–3102. [CrossRef]
- [27] Peng G, Sharshir SW. Progress and performance of multi-stage solar still a review. Desalination 2023;565:116829. [CrossRef]

- [28] Abdullah AS, Hadj-Taieb L, Aljaghtham M, Omara ZM, Essa FA. Enhancing rotating wick solar still performance with various porous breathable belt designs and nanofluid. Case Stud Therm Eng 2023;49:103205. [CrossRef]
- [29] Sathyamurthy R, Ali HM, Said Z, El-Sebaey MS, Gopalsamy S, Nagaraj M, Almasoud N, et al. Enhancing solar still thermal performance: the role of surface coating and thermal energy storage in repurposed soda cans. J Energy Storage 2024;77:109807. [CrossRef]
- [30] Hammoodi KA, Dhahad HA, Alawee WH, Omara ZM. A detailed review of the factors impacting pyramid type solar still performance. Alex Eng J 2023;66:123–154. [CrossRef]
- [31] Singh V, Kumar R, Saxena A, Dobriyal R, Tiwari S, Singh DB. An analytical study on the effect of different photovoltaic technologies on enviro-economic parameter and energy metrics of active solar desalting unit. Energy 2024;294:130851. [CrossRef]
- [32] Hemmatian A, Kargarsharifabad H, Esfahlani AA, Rahbar N, Shoeibi S. Improving solar still performance with heat pipe/pulsating heat pipe evacuated tube solar collectors and PCM: an experimental and environmental analysis. Sol Energy 2024;269:112371. [CrossRef]
- [33] Venkatasamy M, Sivamani S, Venkatesan H, Thangaraj M. Experimental study on productivity enhancement of an improvised inclined solar still. Int J Ambient Energy 2018;39:165–175. [CrossRef]
- [34] Yuvaperiyasamy M, Senthilkumar N, Deepanraj B. Experimental and theoretical analysis of solar still with solar pond for enhancing the performance of sea water desalination. Water Reuse 2023;13:620–633. [CrossRef]
- [35] Saravanan S, Gajalakshmi K, Kumararaja K, Sivaraman B, Raghukandan K. Prediction of aluminium–stainless steel explosive clad strength through machine learning. Sadhana 2023;48:140.

 [CrossRef]
- [36] Kumararaja K, Sivaraman B, Saravanan S. Performance evaluation of hybrid nanofluid-filled cylindrical heat pipe by machine learning algorithms. J Therm Eng 2024;10:286-298.